Efficient thermoelectric materials using nonmagnetic double perovskites with d^0/d^6 band filling

Pablo Villar Arribi,[1,2,3] Pablo García-Fernández,[4] Javier Junquera,[4] and Victor Pardo[1,2,*]

[1] *Departamento de Física Aplicada, Universidade de Santiago de Compostela, E-15782 Santiago de Compostela, Spain*
[2] *Instituto de Investigacións Tecnolóxicas, Universidade de Santiago de Compostela, E-15782 Santiago de Compostela, Spain*
[3] *European Synchrotron Radiation Facility, 71 Avenue des Martyrs, F-38000 Grenoble, France*
[4] *Departamento de Ciencias de la Tierra y Física de la Materia Condensada, Universidad de Cantabria, Cantabria Campus Internacional, Avenida de los Castros s/n, E-39005 Santander, Spain*

(Dated: June 24, 2016)

Efficient thermoelectric materials should present large Seebeck coefficient, high electrical conductivity and low thermal conductivity. An enhanced Seebeck coefficient can be obtained from materials where the Fermi level can be aligned with a large and narrow peak of the density of states, particularly when a substantial band valley degeneracy occurs. A high electrical conductivity comes as a consequence of large conductive hopping paths between the atoms of the material. Both physical quantities can be decoupled and optimized independently if their origins can be ascribed to different sets of bands. Based on these assumptions, double perovskites $A_2BB'O_6$ with d^0/d^6 filling for the B and B' metal cations, respectively, have been considered. They provide a desirable band structure with degenerate B-t_{2g} / B'-e_g bands above the Fermi level together with a low thermal conductivity. We have carried out first-principles simulations for various of these nonmagnetic double perovskites and showed that all of them present a large Seebeck coefficient (consequence of the localized and empty t_{2g} states of the B-cation), and large electrical conductivity due to the more spread unoccupied e_g band of the B' cation. We have seen that if they can be optimally doped, they could show a figure of merit comparable or even higher than the best n-type thermoelectric oxides, such as $SrTiO_3$. Different mechanisms to tune the band structure and enhance the thermoelectric figure of merit are explored, including epitaxial strain, hydrostatic pressure, chemical pressure, and external doping. A fully relaxed structure has also been studied, showing that a realistic calculation is necessary to make accurate predictions, but also proving that the main trends shown throughout the paper remain unchanged.

PACS numbers: 72.20.Pa, 71.20.-b, 72.80.Ga

arXiv:1602.01539v2 [cond-mat.str-el] 23 Jun 2016

I. INTRODUCTION

The quest for new materials with outstanding thermoelectric (TE) properties is one of the cutting-edge research topics nowadays because of its multiple applications: from Peltier cooling to the conversion of waste heat into electricity in order to, for instance, reduce fuel consumption in vehicles. The TE efficiency of these materials can be characterized by a dimensionless TE figure of merit $zT = \sigma S^2 T/\kappa$, where σ is the electrical conductivity, S is the Seebeck coefficient, T is the absolute temperature, and $\kappa = \kappa_e + \kappa_l$ is the thermal conductivity which contains both the electron, κ_e, and lattice, κ_l, contributions.

Improving zT can be achieved combining different strategies. A first choice consists in reducing the total thermal conductivity, which often implies reducing the lattice part. Heat carried by lattice vibrations (phonons in the quantized form) is particularly detrimental to TE performance[1] since the heat backflow leads to a reduction in the temperature gradient required for the TE module to operate. The idea of reducing thermal conductivity while retaining reasonable values for both the electrical conductivity and the Seebeck coefficient lies at the basis of the "phonon-glass, electron-crystal" concept developed by Slack more than twenty years ago.[2,3] This is often carried out by the use of materials with very complex unit cells[4,5] or cage-like compounds in which heavy atoms are enclosed. The rattling of these heavy atoms strongly scatters phonons, specially those with a longer wavelength, that are the most involved in the heat transport, with the corresponding reduction in lattice thermal conductivity. Examples of structures that can lead to excellent TE materials, some of these based on these concepts are skutterudites,[6–8] clathrates,[9] chalcogenides,[10] Zintl-phases,[11] or half-Heusler alloys.[12,13]

A second way to improve the TE figure of merit is to maximize the power factor, defined as the product σS^2, by varying the carrier concentration with different doping levels.[14–16] This approach has its limitations, since the Seebeck coefficient, electrical conductivity, and electronic thermal conductivity are strongly interconnected. Typically, S is small in metals, leading to small power factors. On the other hand, S is large for semiconductors and insulators but σ is lower for them, so the power factor σS^2 is again very small.[17] For a given material, the carrier concentration can be optimized to achieve a good compromise among these quantities in order to enhance the value of the power factor. The values that maximize the power factor are usually of the order of 10^{18}-10^{19} cm^{-3}, typical in extrinsic doped semiconductors and semimetals. However, the interdependency of

the Seebeck coefficient and the electrical conductivity hampers the applicability of this optimization method. A more desirable strategy would require the decoupling of these two quantities.

Since the Seebeck coefficient is directly proportional to the energy derivative of the electronic conductivity at the Fermi energy, E_F, itself related with the density of states (DOS),[18] then the presence of narrow and sharp features of the DOS around E_F can increase the thermopower [see Eq. (2) of Ref. 19]. The idea of tuning the band structure of materials to enhance the thermoelectric figure of merit was proposed by Hicks and Dresselhaus in two milestone works two decades ago.[20,21] Working within a free-electron model, these authors showed how a reduction in the dimensionality of the TE materials could dramatically improve their performance because (i) the electron confinement in low-dimensional systems modifies the shape of the DOS, that displays a staircase-shaped energy dependence with each step being associated with one of the energy states (in 2D), divergence near the bottom of each of the one-dimensional subbands (in 1D) or isolated peaks located at the energy states (in 0D), with large derivatives at the previous particular energy positions, and (ii) the boundaries of the low-dimensional system would increase the scattering of phonons with wavelengths comparable or larger than its spatial dimensions, leading to a considerable reduction of the thermal conductivity.

Another approach to induce peaks in the DOS is the use of materials with strongly correlated electrons. From this perspective, oxides are a very attractive option.[22] Oxygen can be combined with many different cations in relatively simple structures that present very different structural phase-transition sequences involving polar and non-polar distortions; equilibrium phases of insulating, semi-conducting, metallic and even superconducting character; and piezoelectric, ferroelectric, ferromagnetic, multiferroic or TE properties, making them ideal candidates for multifunctional devices. Also, they are stable under ambient conditions and they can be processed on the nanoscale in the form of thin films, nanoparticles, or even nanowires using nowadays standard techniques. The study of TE properties on oxides was boosted after the discovery of a large thermopower in the metallic layered Na_xCoO_2 cobaltates, with zT values up to 1.0 at 800 K.[23–26] This family of materials are composed by triangular planes of CoO_2, where the Co atoms sit inside trigonally distorted edge-sharing octahedra, separated by layers filled with Na^+. Their electronic structure combines two sets of electrons produced by the trigonal splitting of the t_{2g} manifold: delocalized e_g^π and more localized a_{1g} electrons.[27] The former provide a large conductivity, and the latter help increasing the Seebeck coefficient. This, together with their relatively small thermal conductivity, places layered cobaltates as the highest zT recorded for oxides. Other oxides that show large power factors are, e.g. n-type doped $SrTiO_3$ (nominal $3d^0$ electronic configuration) or, more recently CrN (not an oxide, but very close in terms of electronic structure[28] with its nominal $3d^3$ electronic configuration with a full majority-spin t_{2g} band in each site and its naturally occurring electron doping). Both of them have been found to increase its zT dramatically when nanostructured (see Ref. 29 for $SrTiO_3$ and Ref. 30 for CrN). These two systems have in common the occurrence of empty d-bands just above the Fermi energy that yield a set of localized levels that are sensitive to electron doping. Very similar band fillings will be explored in the present work.

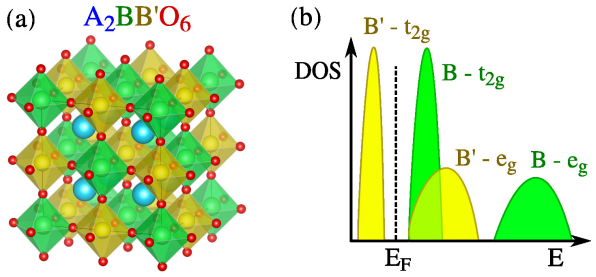

FIG. 1. (Color online) (a) Schematic representation of the $A_2BB'O_6$ double-perovskite structure studied in this work, where A denotes a di- or trivalent cation, while B and B' are transition metal atoms. O atoms are shown in red, A cation in blue, and the B and B' cations are represented by green (dark) and yellow (clear) spheres, with the O octahedra colored accordingly. (b) Scheme of the expected electronic structure configuration, represented by the DOS, for d^0/d^6 band filling of the B (empty d shells, shown in green) and B' (full t_{2g} manifold displayed in yellow) cations, respectively.

Trying to put together all these evidences for oxides and TE materials in general, we have attacked the problem from a different facet: instead of playing with dimensionality, we exploit the very flexible chemical composition that can be found in oxides. We focus on double perovskites of generic chemical formula $A_2BB'O_6$ [see a picture of the well-known structure in Fig. 1(a)], where A is a di- or trivalent cation, while B and B' are different transition metals that are combined in such a way that they have a d^0/d^6 filling. The expected DOS is schematically represented in the cartoon of Fig. 1(b). The B cation has a completely empty d-shell, with a localized t_{2g} band just above the Fermi level. When the system is electron-doped, this band should yield a large thermopower. Assuming that the B' cation is in a low-spin state, it presents a full t_{2g} shell. Due to the presence of a broad empty e_g band just above the Fermi level, a highly conductive hopping path is provided. Besides, low thermal conductivities (compared with $SrTiO_3$ at optimal doping levels) below 1 W $\times$ m^{-1} $\times$ K $^{-1}$ have been reported[31] in other related double-perovskite oxides, and these low values have been related to the double-perovskite structure itself. This encourages to think that if they can be doped at an optimal level, these systems could be potential candidates to become excel-

lent TE materials. To test the validity of the previous hypothesis on the electronic structure, we have carried out first-principles simulations combined with semiclassical Boltzmann computations of the transport quantities.

The rest of the paper is organized as follows. The requirements for the ideal double perovskite are summarized in Sec. II. The methods utilized for the simulations are described in Sec. III. In Sec. IV we present the electronic structures, Seebeck coefficients, electrical conductivities and power factors of different double perovskites, both in the relaxed cubic structures and under biaxial strain, whose application has been already used to modify the band structure and enhance the power factor in other materials.[32–35] We also present other methods to tune the band structure, based on cation intermixing or volume variations, and analyze a more realistic case with a fully relaxed structure. Finally, we compare the results with the best n-type oxide TE material up to date, $SrTiO_3$.

II. SELECTING THE CANDIDATES

The properties that the candidate double-perovskite materials should meet in order to achieve the ideal band structure with the d^0/d^6 filling scheme depicted in Fig. 1(b) can be enumerated as follows. (i) The cation on the B' site must be in a low-spin state to yield a filled t_{2g} shell. For this reason, transition metal elements from the $4d$ and $5d$ rows are selected. (ii) The highly-degenerate electronic configuration at the low electron-doping region which provides the desired scheme for a high Seebeck coefficient requires an empty d-shell in the B-cation site. For the studied compounds, we choose only elements in their most usual valence state, since these materials are ultimately expected to be grown in the laboratory. (iii) We study only ordered double perovskites. This ordered structure is more likely to occur if there is a substantial difference in size and/or valence between the B and B' cations. To ensure that the cubic perovskite structure is preserved (or is at least a good approximation), we also combine elements whose ionic radii fulfill the tolerance factor relation

$$t = \frac{r_{\mathrm{A}} + r_{\mathrm{O}}}{\sqrt{2}(\langle r_{\mathrm{B}} \rangle + r_{\mathrm{O}})} \lesssim 1, \tag{1}$$

where $\langle r_{\mathrm{B}} \rangle$ is the average ionic radii of the B and B' cations, r_{O} is the oxygen's ionic radius and r_{A} is the A cation ionic radius. If the tolerance factor is on the order of 1, the structure tends to be more stable in the cubic phase. In principle, non-cubic perovskites would be useful as well, but a much more complex computational treatment is required due to distortions.

Under these premises, we consider for the B site Ti^{4+}, Nb^{5+}, and Ta^{5+} cations from the $3d$, $4d$, and $5d$ transition metal series, respectively. These are combined with Ir^{3+}, Rh^{3+}, Pt^{4+}, and Pd^{4+} cations for the B' site, from the $4d$ and $5d$ transition metal series. Typical A cations chosen are Sr^{2+} and La^{3+} or an ordered mixture of both.

III. COMPUTATIONAL DETAILS

Electronic band structures are calculated within the density functional theory (DFT)[36,37] framework using the all-electron, full potential code WIEN2K.[38] This package is based on the augmented plane waves plus local orbitals (APW+lo) method.[39]

Typical values for the muffin-tin spheres radii used are (in a.u.): 2.50 for Sr and La; 1.90 for Ta, Rh, Ir, Pd, Pt, Ti, and Nb; and 1.60 for O. In some cases, especially under the most extreme strain conditions that are discussed in Sec. IV B, these radii were further reduced.

Inside the muffin-tin spheres, the mixed APW+lo (where lo stands for local orbital) and LAPW basis set are expanded in spherical harmonics up to $\ell_{\mathrm{max}}^{\mathrm{wf}} = 10$. Nonspherical contributions to the electron density and potential up to $\ell_{\mathrm{max}}^{\mathrm{pot}} = 6$ are used.

In LAPW-based methods, the plane-wave cutoff for the electronic wave functions in the interstitials is controlled by the parameter $R_{\mathrm{min}}^{\mathrm{MT}} \times \mathrm{K}_{\mathrm{max}}$, where $R_{\mathrm{min}}^{\mathrm{MT}}$ is the smallest muffin-tin sphere radius and $\mathrm{K}_{\mathrm{max}}$ is the largest plane wave momentum vector defined by this product. A parameter $R_{\mathrm{MT}} \times \mathrm{K}_{\mathrm{max}} = 7.0$ ensures calculations are converged for the magnitudes presented, in particular optimal volumes and band gaps.

The integrals in reciprocal space are well converged, using a sampling in k-space of $8 \times 8 \times 8$, generated using the modified tetrahedron method.[40] For the computation of the density of states (DOS), a non-self-consistent calculation within a grid of $15 \times 15 \times 15$ is carried out.

The relaxed lattice parameters are obtained within the generalized gradient approximation (GGA), using the exchange and correlation functional proposed by Wu and Cohen.[41] This choice is motivated by the fact that it is known that the Wu and Cohen functional improves the accuracy of the structural properties of bulk ABO_3 ferroelectrics over the most usual GGA's.[42] For each combination of cations, we performed an initial volume optimization within a cubic perovskite structure, and the results on the TE properties are discussed in Sec. IV A. Then, the effect of biaxial strain imposed by a hypothetical substrate is simulated, constraining the length of the lattice vectors along the three cartesian directions in such a way that $a = b \neq c$. Assuming that the in-plane lattice constant, a, is determined by the substrate, then the out-of-plane lattice constant c is relaxed. The results are summarized in Sec. IV B. The possibility of tuning the band structure under hydrostatic pressure is also explored (Sec. IV C 2). In this case, volume reductions are performed decreasing the cubic a lattice parameter retaining the cubic symmetry. Finally, a full relaxation of the atomic structure is studied in Sec. IV D, for which all forces were relaxed below 2.0 mRy/a.u.

Once the atomic structure is determined in every case,

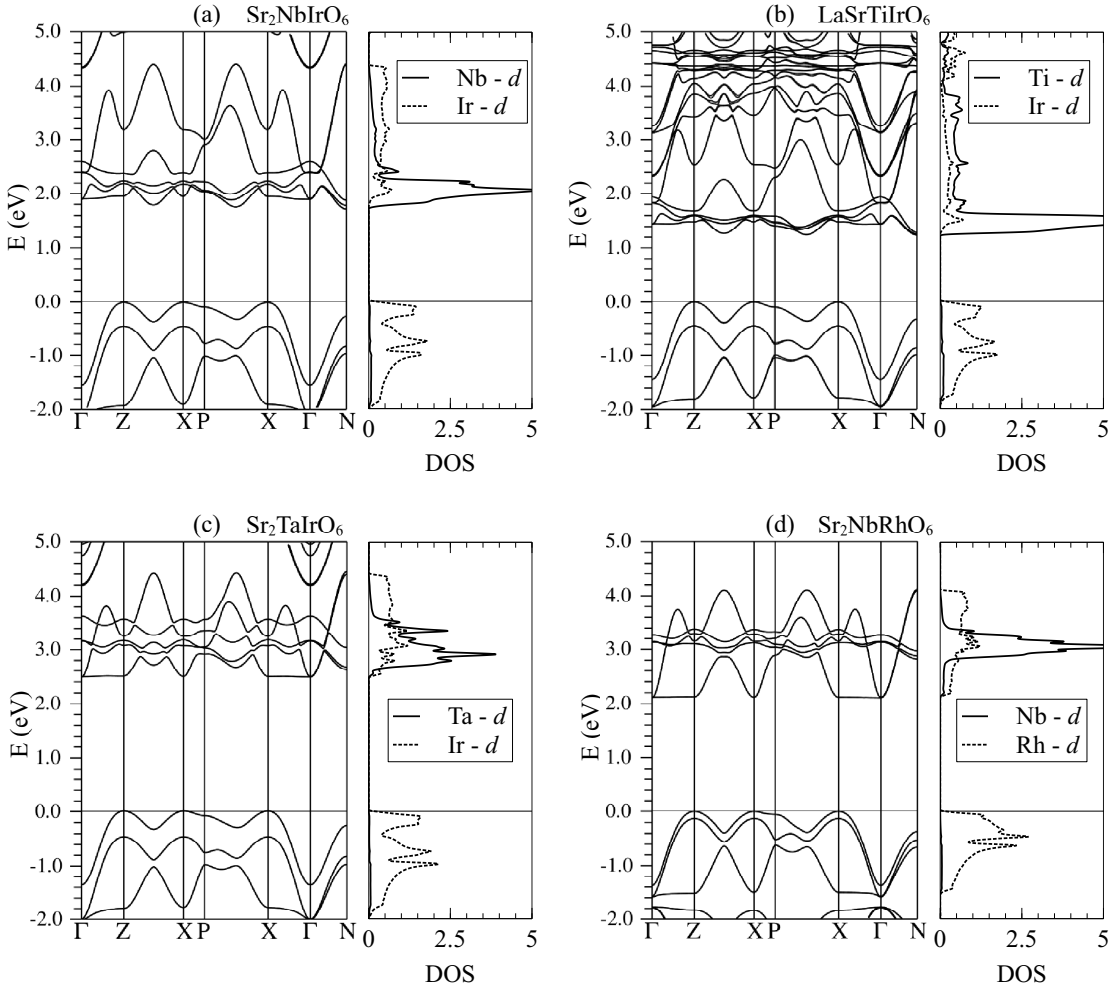

FIG. 2. Band structure (left) and density of states (DOS, right) of (a) Sr_2NbIrO_6, (b) $LaSrTiIrO_6$, (c) Sr_2TaIrO_6 and (d) Sr_2NbRhO_6. In the DOS plots, solid lines represent the projection on the d-shell of the cations at the B-site (supposed to be in a d^0 configuration), and dotted lines on the cations at the B'-site (supposed to be in a d^6 configuration). The zero of the energy is set to the top of the valence bands for all compounds and the scale is the same for all cases. Only the DOS projected on the d electrons are represented as they are the main contributors to the bands that can be accessed by electron doping at the energy range considered here. Units: energies in eV and DOS in states/(eV $\times$ spin).

we have used the Tran-Blaha modified Becke-Johnson (TB-mBJ) semilocal exchange potential for obtaining the band structures,[43] since this functional has been shown to reproduce successfully the band gap for a wide range of semiconductors and oxides,[44,45] $SrTiO_3$ among them.[46] Due to the presence of heavy atoms with $4d$ and $5d$ electrons, spin-orbit interaction effects could be of significance. In order to assess the importance of spin-orbit coupling and eventual modifications of the band structure of these double perovskites, we have performed calculations including this effect in a second variational manner.[47]

An on-site Coulomb repulsion U for the compounds containing La is used to move La-$4f$ empty levels[48,49] away from the Fermi energy. This is motivated by the fact that these orbitals do not participate in the calculation of the transport coefficients,[50,51] which involves only a very narrow energy range related with the d-bands, and its explicit consideration might introduce spurious contributions in the TE phenomena analyzed. This is carried out with the usual LDA+U[52,53] prescription (with an U around 9 eV), where the uncorrelated part of the exchange-correlation is obtained using the TB-mBJ scheme explained above. Realistic inclusion of $4f$ orbitals would require to adequately select U to match the experimental position of these levels in the studied double perovskites, but this is beyond the scope of the current work.

We have estimated the electrical conductivity and the Seebeck coefficient through the semiclassical Boltzmann

theory[18,54] within the constant relaxation time approximation, as implemented in the BoltzTraP code.[50] This implementation relies on the Fourier expansion of the band-energies, provided by a first-principles electronic structure code (wien2k in the present study). In this case, a denser k-mesh of $25 \times 25 \times 25$ is needed to reach convergence for the Fermi-surface integrals involved in the TE quantities presented. Since we are using the simple constant relaxation time approximation, the scope of our paper is to provide on the one hand trends with strain and also a relationship between electronic structure and transport properties. It is not our intent to give accurate values for the optimal doping or Seebeck coefficients, these should be taken with caution when comparing with future experiments.

IV. RESULTS AND DISCUSSION

A. Relaxed case electronic structure

Figure 2 shows the band structures and densities of states (DOS) for some representative double-perovskite cases. It is interesting to compare their basic electronic structure with the rough picture described above as the desired electronic structure in the cartoon of Fig. 1(b). For Sr_2NbIrO_6, Fig. 2(a), narrow Nb t_{2g} bands are just at the bottom of the conduction band, almost degenerate with the wider Ir e_g bands. The same happens with other compounds like $LaSrTiIrO_6$ [Fig. 2(b)] or Sr_2TaIrO_6 [Fig. 2(c)], all of them characterized by the presence of a $5d$ cation, Ir, at the B'-site. However, there are some other cases like Sr_2NbRhO_6 [Fig. 2(d)] which present a slightly shifted band structure, with the unoccupied t_{2g} bands of the d^0 metal lying at the middle of the B'-e_g bands. All in all, the main result that can be drawn is that these double perovskites combine a localized B-t_{2g} band and a more delocalized B'-e_g band that lie roughly in the same energy window. The actual details of band orderings depend on the particular atomic configuration of the system but, to a first approximation, we find that it is possible to obtain an electronic structure similar to the one sketched in Fig. 1(b).

In order to analyze the TE properties of these double perovskites, we show in Fig. 3 the power factor divided by the relaxation time as a function of the carrier concentration for three different temperatures. The calculations are performed within the semiclassical Boltzmann theory with two approximations: (i) the constant relaxation time, and (ii) the "rigid band approach" that assumes that the band structure does not change with temperature or doping and, therefore, it is fixed independently of the chemical potential. Despite the effect that the energy, temperature or doping dependence of the relaxation time may have on the final figure of merit of the material,[55] we want to stress in this point the importance of having an appropriate electronic structure which can be easily tuned by different means, as it happens in these compounds. The values of σ and thermopower presented are the average value of the diagonal components of the TE tensors. Due to the cubic symmetry of the system, this is a very representative quantity. The main results are: (i) We observe that for all compounds including Ir, the optimal carrier concentration for a maximal power factor and optimal TE performance is approximately $n = 10^{21}$ cm^{-3}, while for those double perovskites which do not include Ir, the maximum is at lower carrier concentrations around $n = 10^{20}$ cm^{-3}. (ii) These optimal doping levels are almost temperature independent; only small deviations of the order of 10% are observed as temperature is increased. (iii) The maxima of the power factor at optimal doping are substantially enhanced with temperature, increasing by about 70% from 300 K to 700 K. The origin for this behaviour can be traced back to the band structures shown in Fig. 2, where it can be seen how the Ir-based compounds present a band degeneracy at the bottom of the conduction band formed by the Ir e_g and Ti/Nb/Ta t_{2g} bands. Such degeneracy is intimately related to an enlarged power factor and a higher optimal carrier concentration. The relationship between large band valley degeneracy and enhancement of the TE properties is well known,[56] and our results confirm that this is possible to obtain with these double perovskites to some extent.

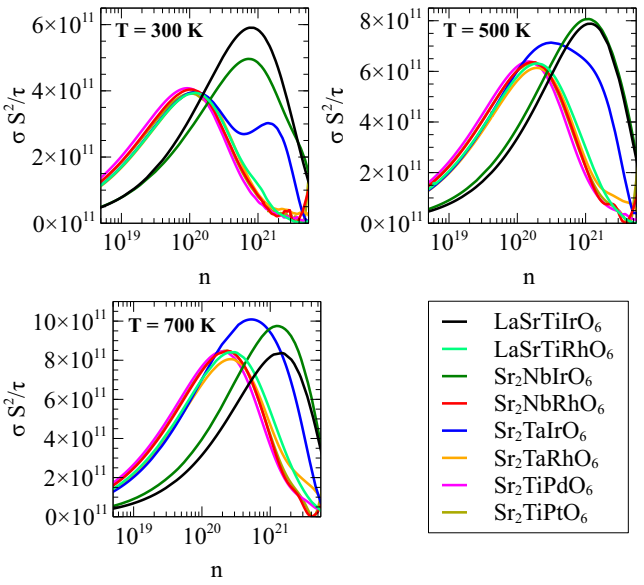

FIG. 3. (Color online) Power factor divided by the scattering time for all studied compounds at three different temperatures as a function of carrier concentration. Units: power factor over relaxation time in W/(mK^{-2}s), carrier densities in cm^{-3}.

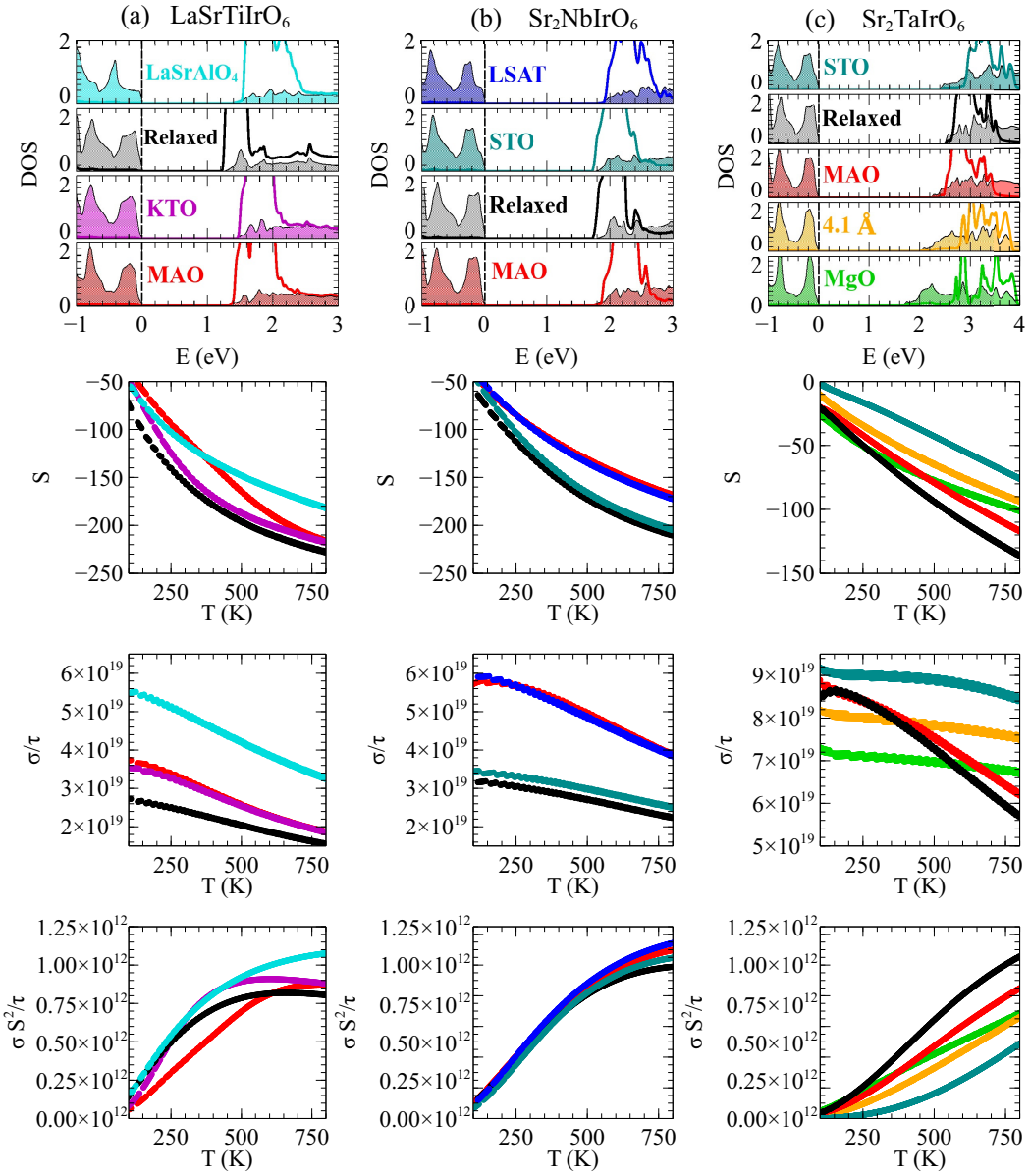

FIG. 4. (Color online). Density of states [DOS, in states/(eV × spin), top row], and temperature dependence of the Seebeck coefficient (S, in μV/K, second row), electrical conductivity over relaxation time [σ/τ, in $1/(\Omega \times m \times s)$, third row], and power factor over relaxation time [$\sigma S^2/\tau$, in W/(m × K ^{2}× s), bottom row] of (a) $LaSrTiIrO_6$, (b) Sr_2NbIrO_6 and (c) Sr_2TaIrO_6. Different strains have been simulated by setting the lattice parameter a to the experimental value of $LaSrAlO_4$ (light blue), LSAT (dark blue), STO (dark green), KTO (magenta), MAO (red), MgO (light green), and with a value of $a = 4.10$ Å(yellow). DOS for the relaxed lattice constant within the cubic symmetry of each compound are shown in grey. Shaded DOS corresponds to the projection on the d-shell of the B'-cation (Ir in the presented examples, assumed to be in a d^6 configuration). Projections on the d-shell of the B-cations (narrower t_{2g} bands) are represented by a solid line. DOS panels over (below) the relaxed plot means compressive (expansive) epitaxial strain. The zero of the energy is set to the top of the valence bands.

B. Tuning the band structure by biaxial strain in the ab-plane

It has been demonstrated theoretically[20,21,29] and also tested experimentally[57,58] how quantum confinement and low-dimensionality could enhance the TE figure of merit of a system. Also, strain has been found to play a role in decoupling the different transport coefficients involved in TE efficiency, which are usually inter-related.[32–35] Thin films of similar double perovskites have been grown routinely over different substrates.[59,60] Thus, it is plausible to explore the effects of biaxial strain (which is achieved

by means of epitaxial growth of thin films over substrates with a different lattice parameter) on these compounds. We can theoretically analyze the effects of both compressive and tensile strain in the band structure of these materials by simply imposing the in-plane a lattice parameter and relaxing the c out-of-plane lattice constant keeping the constraint of a tetragonal symmetry. By studying the general changes in the electronic structure and TE properties we can try to generalize and construct a recipe to improve the TE response of these double perovskites.

For a better comparison with experiments, we have selected the a lattice constant corresponding to the experimental value of different commonly used substrates, that cover a wide range of a lattice constants: $LaSrAlO_4$ ($a_{LaSrAlO_4}$= 3.755 Å), $(LaAlO_3)_{0.3}(Sr_2TaAlO_6)_{0.7}$ (LSAT, a_{LSAT} = 3.868 Å), $SrTiO_3$ (STO, a_{STO} = 3.905 Å), $KTaO_3$ (KTO, a_{KTO} = 3.989 Å), $MgAl_2O_4$ (MAO, a_{MAO} = 4.041 Å), MgO (a_{MgO} = 4.212 Å), and another set of calculations with $a = 4.1$ Å to fill the gap between MAO and MgO.

The epitaxial strain changes both the position of the center and the widths of the bottom conduction bands in systems with octahedral symmetries, such as the double perovskites considered here. For t_{2g} bands coming from the B cation, on the one hand, a compressive epitaxial strain produces an elongation of the oxygen octahedra along the c direction that stabilizes the d orbitals with z components, so the center of the respective bands (the d_{xz} and d_{yz} doublet) are positioned lower in energy than the d_{xy} singlet. Moreover, compressive strain reduces the distance between the atoms in the ab plane and produces larger overlap between the orbitals directed in the plane perpendicular to the strain axis (d_{xy} and $d_{x^2-y^2}$), so the width of the corresponding bands increases. On the other hand, a tensile epitaxial strain produces a compression of the octahedra along the c-direction, that will place the d orbitals with z components higher in energy.[61] In this case, the bands with major character from orbitals with z component are wider.

A similar effect occurs for the B'-e_g bands: tensile (compressive) strain lowers the $d_{x^2-y^2}$ (d_{z^2}) band and band widths get enlarged for the in-plane (out-of-plane) orbital when compressive (tensile) strain is applied. All these effects combined lead to different band displacements that move in different directions when epitaxial strains are applied. The main results are summarized for selected compounds in Fig. 4.

In those cases in which the involved B'-e_g manifold is lower in energy than the B-t_{2g} manifold, such as $LaSrTiIrO_6$ over $LaSrAlO_4$ substrate [Fig. 4(a)], or Sr_2NbIrO_6 over LSAT or MAO substrates [Fig. 4(b)] no drastic effect is observed in the Seebeck coefficient by applying strain (sometimes it gets even slightly reduced because of the wider B-t_{2g} bands). However electrical conductivity in those cases increases to even 2 times the value for the relaxed case within the cubic symmetry (from 2.2×10^{19} to 4.0×10^{19} $1/(\Omega \times m \times s)$ at 800 K for Sr_2NbIrO_6 [Fig. 4(b)]). The result is an enhanced power factor that takes place together with a large degeneracy at the bottom of the conduction band. We present these TE properties obtained at $n = 10^{21}$ cm^{-3} for the three materials appearing in Fig. 4. Depending on the compound, the optimal carrier concentration could vary, but trends are consistent in the 10^{18} - 10^{21} cm^{-3} range. It is not the objective of this work to provide accurate values of the optimal doping. Band structure tuning by shifting bands and modifying their band widths by applying strain is most effective when the bottom of the B-t_{2g} and B'-e_g bands get close in energy, as can be clearly seen for $LaSrTiIrO_6$ [Fig. 4(a)] and Sr_2NbIrO_6 [Fig. 4(b)]. One can also notice in these two panels that if the B-t_{2g} band gets occupied first (at this electron-doping level we are considering) the electrical conductivity gets drastically reduced and thus the power factor is lower [in Fig. 4(a) for all substrates except for $LaSrAlO_4$ and in Fig. 4(b) for STO and the relaxed case within the cubic symmetry].

In Fig. 4(c) we see the results for Sr_2TaIrO_6, which confirms the trend that the presence of a lower lying B'-e_g band is necessary for an enlarged power factor to occur. The other important fact seen here is that the wider the t_{2g} bands, the lower the Seebeck coefficient is, which is not a surprising effect. In some cases, even biaxial strain does not enhance the TE properties since the relaxed case within the cubic symmetry already presents an optimal configuration.

For the other compounds (not shown) strain does not play a major role. In the limit in which the B-t_{2g} bands lie in the middle of the broader B'-e_g bands, the effect is very small because it does not largely affect the doping region where large band valley degeneracy occurs. The value of the power factor obtained for the corresponding double perovskites is lower than in the other compounds because the Seebeck coefficient is not so large. Even when biaxial strain is applied, we do not observe a significant improvement of the TE properties.

We conclude that an initial configuration with the B-t_{2g} and B'-e_g bands being both at the bottom of the conduction band is required for having good TE properties in these systems, and that in those cases it is possible to tune them by means of biaxial strain.

C. Other methods to tune the band structure

Besides the application of biaxial strains imposed by epitaxial growth, we have examined three other mechanisms to modify the electronic band structure in order to enhance the TE performance: the effect of using more compact d-states considering atoms of the 3d-row, the use of hydrostatic pressure to reduce the unit-cell volume and change the distance between atoms, and chemical substitution to induce a "chemical pressure" effect. The main results are explained in the following three subsections.

1. Spatial range of the d-orbitals

The effect of the extension of the d orbitals of the B- and B'-cations and the corresponding change in hybridizations has been studied by replacing the previously considered atoms in the $4d/5d$-row by transition metal atoms of the $3d$ row. For this purpose we have chosen La_2TiFeO_6. The existence of ordered cationic structures in this compound can be presumed by the large valence difference. The calculation converges nicely to a $Ti^{4+}(d^0)/Fe^{2+}(d^6)$, where Fe^{2+} is in a low-spin state with a full t_{2g} shell, just like every other compound we have examined previously in this study. We immediately observe that even though the Seebeck coefficient (not shown) remains as large as for the other double perovskites presented, the electrical conductivity is at least one order of magnitude lower than the previous cases. The driving force responsible for this reduction can be ascribed to the more localized character of Fe $3d$-orbitals compared with $4d$ or $5d$ orbitals. The compactness of the d-orbitals makes the hopping between Fe and O lower than the corresponding hopping due to a $4d/5d$ metal. The band structure (not shown) presents the Fe e_g bands above the Ti t_{2g} bands, so the conduction mediated by the e_g bands (which worked in other compounds) is not active in this case, and thus the electrical conductivity is reduced. For these reasons, we have not considered further combinations with $3d^0/3d^6$ transition metal cations and focused only on the combination of $4d/5d$ elements at the B- and B'-sites.

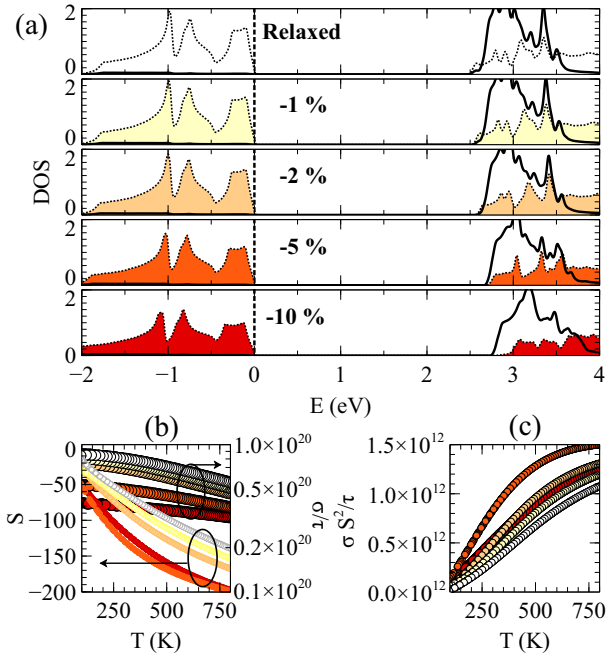

FIG. 5. (Color online) Density of states, thermopower, electrical conductivity and power factor of Sr_2TaIrO_6 at different unit-cell volumes. The color sequence follows from white for the relaxed case in the absence of pressure, to red for the case under the highest pressure (larger volume reduction). Corresponding values of volume reductions are indicated on the top panel. Meaning of lines, symbols and units as in Fig. 4. The electrical conductivity divided by the relaxation time is represented in logarithmic scale.

2. Hydrostatic pressure

We have also studied the possibility of enhancing the TE properties by means of the application of an external hydrostatic pressure. The most important effect induced by pressure is the reduction of the unit cell volume, that is assumed to remain in a cubic symmetry. The structural changes and the concomitant smaller metal-oxygen distances modify the electronic band structure of the double perovskites accordingly. In particular, the crystal field splitting between t_{2g} and e_g levels will be enhanced as pressure is increased. This translates into a lower positioning of the B-t_{2g} bands with respect to the B'-e_g bands that are shifted upwards in the conduction band.

As a test case, we have studied the effect of hydrostatic pressure on Sr_2TaIrO_6, with volume reductions up to 10 % which would correspond to external pressures of about 27 GPa. In this double perovskite, at the relaxed cubic structure in the absence of external pressure, the bottom of the narrow Ta t_{2g} bands are located at the same energy as the bottom of the more widely spread Ir e_g manifold [see DOS at the top of Fig. 5(a)]. Thus, it is a good example where the evolution of these bands with volume variation can be studied. When pressure is applied and the unit cell volume is reduced, the crystal field gap between the t_{2g} and the e_g bands for each atom becomes larger, as it happens also with the width of each of these bands [Fig. 5(a)]. However, both variations are not dramatic, significant changes are only expected if the initial positioning of the bottom of the t_{2g} and e_g bands is really close.

Regarding the transport properties [Fig. 5(b)]: on the one hand, the Seebeck coefficient is enlarged (in absolute value) when the degeneracy at the bottom of the conduction band is maximal. On the other hand, the electrical conductivity is reduced when the volume decreases, i.e. when the system tends to have the more localized Ta t_{2g} bands occupied first, instead of the more spread Ir e_g ones. Combining all these effects [Fig. 5(c)], the higher power factor occurs for a volume reduction of 5% in the unit cell, equivalent to a pressure of 11 GPa.

Again, the final conclusion is that if the involved bands are already close to the optimal band structure configuration, an enhancement of the TE response can be achieved by means of a reasonable volume reduction.

3. Chemical pressure

Volume reductions can also be realized by changing the size of the A cation (so-called chemical pressure). We

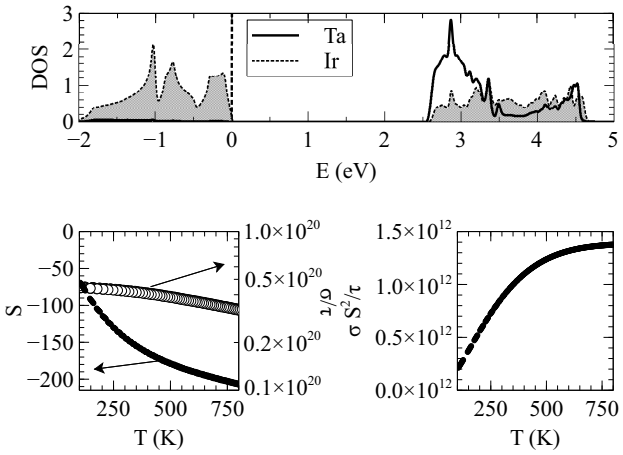

FIG. 6. Electronic structure and thermoelectric properties of Ca_2TaIrO_6. When compared to Sr_2TaIrO_6 under pressure, the tendency towards enhanced thermoelectric properties at lower volumes is retained. Meaning of lines, symbols and units as in Fig. 4. The electrical conductivity divided by the relaxation time is represented in logarithmic scale.

have explored this possibility replacing Sr^{2+} (ionic radius: 1.44 Å) by smaller Ca^{2+} (ionic radius: 1.34 Å) in the double perovskite studied in the previous subsection. This substitution immediately reduces the lattice parameter of the hypothetical cubic phase, that changes from 3.975 Å in Sr_2TaIrO_6 to 3.939 Å in Ca_2TaIrO_6 (volume reduction of 2.7 %).

If we look at the electronic structure and transport properties of Ca_2TaIrO_6 (Fig. 6) we can see that the values for the Seebeck, electrical conductivity, and power factor are essentially the same as the ones for Sr_2TaIrO_6 with a 5% volume reduction. In other words, the chemical substitution (even without applying any external pressure) produces the same effects as the unit cell shrinking that optimized the TE figure of merit.

The main drawback of this approach is that the theoretical tolerance factor [Eq. (1)] is $t = 0.948$ for this compound, so we cannot assume that cubic symmetry will be preserved. Therefore, we acknowledge that these particular calculations could be overestimating the real values for the TE properties. More complete and computationally demanding simulations would be required to check these results, involving a full relaxation of the lattice and atomic positions.

D. Full relaxation

For completeness, we have performed a full relaxation of the double-perovskite structure for one particular case to study its possible effects, even though a comprehensive study is beyond the scope of this paper. We have studied the compound Sr_2NbIrO_6 under different strains. It presents an electronic structure close to the ideal configuration and a tolerance factor of $t = 0.98$. Tilted octahedra result from this structural relaxation. This influences directly the electronic structure and as a consequence, the TE properties of the system. Even though the unit cell preserves a global cubic symmetry, the local environments for the cations become tetragonally distorted.

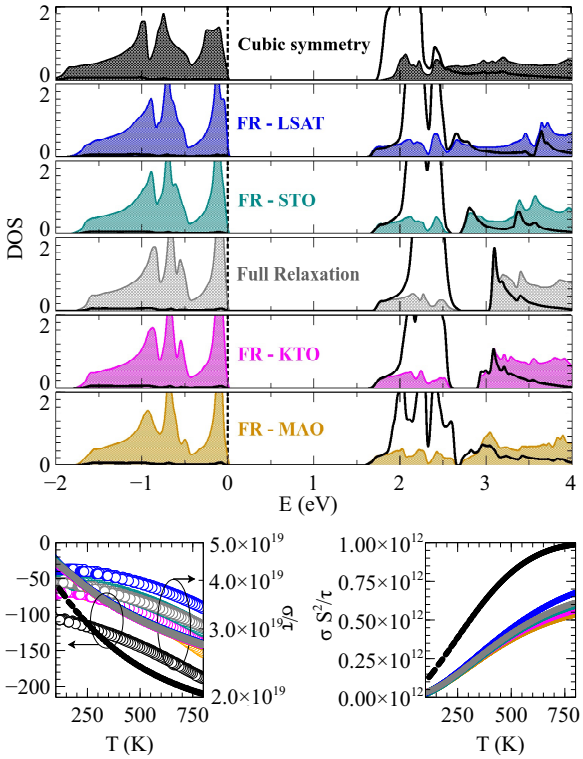

FIG. 7. Electronic structure and thermoelectric properties of Sr_2NbIrO_6 for the cubic structure (black), for the fully relaxed structure (grey), and for the fully relaxed structure plus strain in the *ab*-plane (colors). In both cases, solid black lines represent the Nb *d* bands, meanwhile the shaded density of states represents the Ir *d* bands.

We can see these differences in Fig. 7, in which a comparison between the cubic symmetry case and the fully-relaxed case under different strains is shown. Comparing the cubic-symmetry case with the fully relaxed case without strain, the most notorious effect is the splitting of the Ir e_g manifold. The degeneracy existing within these levels as a consequence of the local tetragonal symmetry is lifted by octahedral rotations. This directly affects the electrical conductivity of the system, since the hopping channel is substantially modified.

For all cases containing a full relaxation, a lower (and almost similar) Seebeck coefficient is present. This is due to the always low-lying Ir e_g which, as we previously discussed, leads to a reduced TE power. A higher electrical conductivity happens in the case of a fully relaxed structure with the substrate LSAT (data in blue in Fig. 7). The e_g bands of Ir (which in this case are not split) provide a wider hopping channel since they are lower in

energy than the Nb t_{2g} bands. Comparing this case with the one with cubic symmetry which also presents degenerate e_g bands (data in black in Fig. 7) one can see the difference between the Seebeck coefficient and the electrical conductivity for both cases. The difference in the electrical conductivity is explained as before, taking into account which hopping path is activated first: the Ir e_g bands in the case of a fully relaxed structure with LSAT and the Nb t_{2g} bands in the case of cubic symmetry. This results in a higher electrical conductivity in the first case. However the Seebeck coefficient is lower in the case of the LSAT substrate because there is no peak in the density of states close to the bottom of the conduction bands, which happens in the case of cubic symmetry.

We are able to obtain a power factor for a fully relaxed structure on the order of 65-70% the value of the power factor in the simplified cubic case. With this result, we want to stress that if one wants to compute the electronic structure of a real compound in a double-perovskite structure, it is necessary to include a full relaxation of the structure, since the transport coefficients are quite sensitive to small changes in the atomic positions. However, the main picture on how the ideal electronic structure would look like does not change, and the main effects discussed throughout the text remain the same. Other calculations in similar systems involving full structural relaxations also retain a large TE efficiency.[62]

E. Comparison with $SrTiO_3$

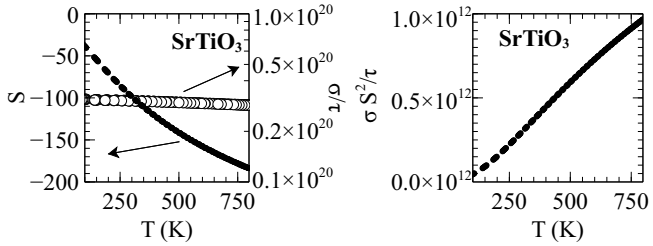

FIG. 8. Thermoelectric properties for $SrTiO_3$. The electrical conductivity divided by the relaxation time is represented by bigger circles and its corresponding axis is in logarithmic scale. Units as in previous figures.

In order to gauge the importance of the enhancements of the TE performance obtained with the tuning of the band structure mechanisms explained in Sec. IV, we have carried out calculations for bulk $SrTiO_3$ (STO), one of the best n-type oxide TE materials found up-to-date.[14–16,29,46] Figure 8 shows the DOS and the TE properties. The values of the Seebeck coefficient match the experimentally observed ones[14–16] by several authors at the optimal carrier concentration (10^{21} cm^{-3}). Since the basic electronic structure is very similar, this constitutes a strong validation of our calculations for the double perovskites presented so far.

If we compare the results for double perovskites with the ones with STO, we can observe that the values for the Seebeck coefficient are, in some cases like $LaSrTiIrO_6$ [Fig. 4(a)], larger that those for STO. The electrical conductivity for these double perovskites is of the same order of magnitude or even higher than that of STO [see, for example, $LaSrTiIrO_6$ on KTO in Fig. 4(a) or Sr_2TaIrO_6 in Fig. 4(c)], assuming that the scattering time remains similar for both systems, which seems a reasonable premise.

But what makes them ultimately very interesting materials is their very low thermal conductivity compared with that of STO. At the optimal doping regime for these compounds, thermal conductivities below 1 W $\times$ m^{-1} $\times$ K $^{-1}$ have been reported[31] for double perovskites, while in STO typical values are easily above 3 W $\times$ m^{-1} $\times$ K $^{-1}$. This can provide a thermoelectric figure of merit up to 3 times larger that that of STO, making these compounds strong candidates for being good TE materials.

V. SUMMARY

We have studied various nonmagnetic oxides in a double-perovskite structure, with a d^0/d^6 ionic configuration combining transition metals from different series. These compounds show a very large Seebeck coefficient, comparable with the largest values calculated for the best TE oxides at reasonable electron-doping levels. The driving force for the large S is the existence of a peak in the DOS coming from the empty t_{2g} bands of one of the cations at the B-site. Our simulations show that the electrical conductivity can be improved by the introduction of broad e_g bands from $4d/5d$ cations. Even more, the band structure can be tuned applying epitaxial strain, so the power factor can be enhanced by up to a 30% with respect to the relaxed cases within the cubic symmetry in some compounds, achieving values even higher than other similar oxides like $SrTiO_3$. This, combined with experimental evidences[31] showing that several double perovskites have lower ($\sim$ 3 times) thermal conductivity than $SrTiO_3$[14–16] at the optimal carrier concentrations makes these materials potential candidates to become (when optimally doped) good thermoelectrics.

In a more general context, we have shown through first-principles calculations the effectiveness of the combination of a highly degenerate band structure around the Fermi level with a more spread e_g band which provides good electrical conductivity together with a narrower and sharp t_{2g} band to optimize the Seebeck coefficient. The crucial point is to have the maximum degeneracy possible at the bottom of the conduction band (if electron doping is considered, as we have done here) but with a lower lying e_g band providing the power factor enhancement. Our calculations show that this configuration optimizes the TE power factor in this kind of systems, and whenever it does not happen as a natural configuration, it can be achieved effectively by means of biaxial strain and/or volume reduction, if the starting band structure is suffi-

ciently close to the "ideal" one.

We also want to stress that in order to make predictions about any specific compound which is proposed here, one should perform a calculation including a full relaxation of the atomic structure, which could introduce deviations from the ideal configuration (such as distorted or rotated octahedra) that would drive to slightly different results coming from a modified electronic structure. Nevertheless, one could find a compound in which a full relaxation of the structure locates the e_g and t_{2g} bands in the correct place with respect to each other. Then strain, volume reduction, or some of the other methods discussed throughout the text can be used to precisely tune the band structure and reach the optimal TE efficiency.

ACKNOWLEDGMENTS

PVA and VP thank the Xunta de Galicia for financial support through project EM 2013/037. VP, PGF and JJ acknowledge financial support from the Spanish Ministery of Economy and Competitiveness through the MINECO Grants No. MAT2013-44673-R (VP), and No. FIS2012-37549-C05-04 (PGF and JJ). VP and PGF also acknowledge funding from the Ramón y Cajal Fellowship RYC-2011-09024 and RYC-2013-12515, respectively.

* victor.pardo@usc.es

[1] D. J. Singh and I. Terasaki, Nat. Mater. **7**, 616 (2008).
[2] G. A. Slack, "Handbook of thermoelectrics," (CRC Press, Boca Raton, Florida, 1995).
[3] M. Beekman, D. T. Morelli, and G. S. Nolas, Nat. Mater. **14**, 1182 (2015).
[4] G. J. Snyder and E. S. Toberer, Nat. Mater. **7**, 105 (2008).
[5] G. S. Nolas, J. Poon, and M. Kanatzidis, MRS Bulletin **31**, 199 (2006).
[6] B. C. Sales, D. Mandrus, and R. K. Williams, Science **272**, 1325 (1996).
[7] D. J. Singh and I. I. Mazin, Phys. Rev. B **56**, R1650 (1997).
[8] V. Keppens, D. Mandrus, B. C. Sales, B. C. Chakoumakos, P. Dai, R. Coldea, M. B. Maple, D. A. Gajewski, E. J. Freeman, and S. Bennington, Nature (London) **395**, 876 (1998).
[9] A. Saramat, G. Svensson, A. E. C. Palmqvist, C. Stiewe, E. Mueller, D. Platzek, S. G. K. Williams, D. M. Rowe, J. D. Bryan, and G. D. Stucky, J. Appl. Phys. **99**, 023708 (2006).
[10] M.-R. Gao, Y.-F. Xu, J. Jiang, and S.-H. Yu, Chem. Soc. Rev. **42**, 2986 (2013).
[11] S. M. Kauzlarich, S. R. Brown, and G. Jeffrey Snyder, Dalton Trans. , 2099 (2007).
[12] Q. Shen, L. Chen, T. Goto, T. Hirai, J. Yang, G. P. Meisner, and C. Uher, Appl. Phys. Lett. **79**, 4165 (2001).
[13] S. R. Culp, J. W. Simonson, S. J. Poon, V. Ponnambalam, J. Edwards, and T. M. Tritt, Appl. Phys. Lett. **93**, 022105 (2008).
[14] S. Ohta, T. Nomura, H. Ohta, and K. Koumoto, J. Appl. Phys. **97**, 034106 (2005).
[15] S. Ohta, T. Nomura, H. Ohta, M. Hirano, H. Hosono, and K. Koumoto, Appl. Phys. Lett. **87**, 092108 (2005).
[16] H. Muta, K. Kurosaki, and S. Yamanaka, J. Alloy Compd. **350**, 292 (2003).
[17] D. W. Bruce, D. O'Hare, and R. I. Walton, *Functional oxides* (John Wiley and Sons, Chichester, West Sussex, 2010).
[18] N. W. Ashcroft and N. D. Mermin, *Solid State Physics* (Saunders College Publishing, Philadelphia, 1976).
[19] J. P. Heremans, V. Jovovic, E. S. Toberer, A. Saramat, K. Kurosaki, A. Charoenphakdee, S. Yamanaka, and G. J. Snyder, Science **321**, 554 (2008).
[20] L. D. Hicks and M. S. Dresselhaus, Phys. Rev. B **47**, 12727 (1993).
[21] L. D. Hicks and M. S. Dresselhaus, Phys. Rev. B **47**, 16631 (1993).
[22] S. Hébert, D. Berthebaud, R. Daou, Y. Bréard, D. Pelloquin, E. Guilmeau, F. Gascoin, O. Lebedev, and A. Maignan, J. Phys.: Condens. Matter **28**, 013001 (2015).
[23] I. Terasaki, Y. Sasago, and K. Uchinokura, Phys. Rev. B **56**, R12685 (1997).
[24] W. Koshibae, K. Tsutsui, and S. Maekawa, Phys. Rev. B **62**, 6869 (2000).
[25] S. Hébert, S. Lambert, D. Pelloquin, and A. Maignan, Phys. Rev. B **64**, 172101 (2001).
[26] D. J. Singh, Phys. Rev. B **61**, 13397 (2000).
[27] T. Yamamoto, K. Uchinokura, and I. Tsukada, Phys. Rev. B **65**, 184434 (2002).
[28] A. S. Botana, F. Tran, V. Pardo, D. Baldomir, and P. Blaha, Phys. Rev. B **85**, 235118 (2012).
[29] H. Ohta, S. Kim, Y. Mune, T. Mizoguchi, K. Nomura, S. Ohta, T. Nomura, Y. Nakanishi, Y. Ikuhara, M. Hirano, *et al.*, Nat. Mater. **6**, 129 (2007).
[30] C. X. Quintela, J. P. Podkaminer, M. N. Luckyanova, T. R. Paudel, E. L. Thies, D. A. Hillsberry, D. A. Tenne, E. Y. Tsymbal, G. Chen, C.-B. Eom, *et al.*, Adv. Mater. **27**, 3032 (2015).
[31] R. Takahashi, R. Okazaki, Y. Yasui, I. Terasaki, T. Sudayama, H. Nakao, Y. Yamasaki, J. Okamoto, Y. Murakami, and Y. Kitajima, J. Appl. Phys. **112**, 073714 (2012).
[32] P. L. Bach, J. M. Vila-Fungueiriño, V. Leborán, E. Ferreiro-Vila, B. Rodríguez-González, and F. Rivadulla, APL Mat. **1**, 021101 (2013).
[33] V. Pardo, A. S. Botana, and D. Baldomir, Phys. Rev. B **87**, 125148 (2013).
[34] Y. Saeed, N. Singh, and U. Schwingenschlögl, Appl. Phys. Lett. **104**, 033105 (2014).
[35] Y. Saeed, N. Singh, and U. Schwingenschlögl, Appl. Phys. Lett. **105**, 031915 (2014).
[36] P. Hohenberg and W. Kohn, Phys. Rev. **136**, B864 (1964).
[37] W. Kohn and L. J. Sham, Phys. Rev. **140**, A1133 (1965).
[38] K. Schwarz and P. Blaha, Comp. Mater. Sci. **28**, 259 (2003).
[39] E. Sjöstedt, L. Nordström, and D. J. Singh, Solid State Commun. **114**, 15 (2000).
[40] P. E. Blöchl, O. Jepsen, and O. K. Andersen, Phys. Rev. B **49**, 16223 (1994).
[41] Z. Wu and R. E. Cohen, Phys. Rev. B **73**, 235116 (2006).

[42] T. Nishimatsu, M. Iwamoto, Y. Kawazoe, and U. V. Waghmare, Phys. Rev. B **82**, 134106 (2010).
[43] F. Tran and P. Blaha, Phys. Rev. Lett. **102**, 226401 (2009).
[44] D. Koller, F. Tran, and P. Blaha, Phys. Rev. B **83**, 195134 (2011).
[45] H. Dixit, R. Saniz, S. Cottenier, D. Lamoen, and B. Partoens, J. Phys.: Condens. Mat. **24**, 205503 (2012).
[46] A. Sarantopoulos, E. Ferreiro-Vila, V. Pardo, C. Magén, M. H. Aguirre, and F. Rivadulla, Phys. Rev. Lett. **115**, 166801 (2015).
[47] D. J. Singh and L. Nordstrom, *Planewaves, Pseudopotentials, and the LAPW method* (Springer Science & Business Media, 2006).
[48] V. I. Anisimov, F. Aryasetiawan, and A. I. Lichtenstein, J. Phys.: Condens. Mat. **9**, 767 (1997).
[49] R. Gillen, S. J. Clark, and J. Robertson, Phys. Rev. B **87**, 125116 (2013).
[50] G. K. H. Madsen and D. J. Singh, Comp. Phys. Comm. **175**, 67 (2006).
[51] T. J. Scheidemantel, C. Ambrosch-Draxl, T. Thonhauser, J. V. Badding, and J. O. Sofo, Phys. Rev. B **68**, 125210 (2003).
[52] V. I. Anisimov, J. Zaanen, and O. K. Andersen, Phys. Rev. B **44**, 943 (1991).
[53] A. G. Petukhov, I. I. Mazin, L. Chioncel, and A. I. Lichtenstein, Phys. Rev. B **67**, 153106 (2003).
[54] J. M. Ziman, *Principles of the theory of solids* (Cambridge University Press, Cambridge, 1972).
[55] J. Zhou, R. Yang, G. Chen, and M. S. Dresselhaus, Phys. Rev. Lett. **107**, 226601 (2011).
[56] Y. Pei, X. Shi, A. LaLonde, H. Wang, L. Chen, and G. J. Snyder, Nature (London) **473**, 66 (2011).
[57] A. I. Boukai, Y. Bunimovich, J. Tahir-Kheli, J.-K. Yu, W. A. Goddard III, and J. R. Heath, Nature (London) **451**, 168 (2008).
[58] A. I. Hochbaum, R. Chen, R. D. Delgado, W. Liang, E. C. Garnett, M. Najarian, A. Majumdar, and P. Yang, Nature (London) **451**, 163 (2008).
[59] H. Guo, J. Burgess, S. Street, A. Gupta, T. G. Calvarese, and M. A. Subramanian, Appl. Phys. Lett. **89**, 022509 (2006).
[60] T. Manako, M. Izumi, Y. Konishi, K.-I. Kobayashi, M. Kawasaki, and Y. Tokura, Appl. Phys. Lett. **74**, 2215 (1999).
[61] A. Valionis, "Epitaxial growth of complex metal oxides," (Elsevier, Cambridge, 2015).
[62] K. F. Garrity, arxiv/1601.01622 (2016).